Monitoring of Biofilm Formation on Different Material Surfaces of Medical Devices using Hyperspectral Imaging Method

Do-Hyun Kim[1], Moon S. Kim[2], and Jeeseong Hwang[3]
[1]US Food and Drug Administration, Silver Spring, MD 20993
[2]U.S. Department of Agriculture, Beltsville, MD 20705
[3]National Institute of Standards and Technology, Gaithersburg, MD 20899

Abstract: Contamination of the inner surface of indwelling (implanted) medical devices by microbial biofilm is a serious problem. Some microbial bacteria such as *Escherichia coli* form biofilms that lead to potentially life-threatening infections. Other types of medical devices such as bronchoscopes and duodenoscopes account for the highest number of reported endoscopic infections where microbial biofilm is one of the major causes for these infections. We applied a hyperspectral imaging method to detect biofilm contamination on the surface of several common materials used for medical devices. Such materials include stainless steel, titanium, and stainless-steel-titanium alloy. Potential uses of hyperspectral imaging technique to monitor biofilm attachment to different material surfaces are discussed.

Key words: Hyperspectral imaging, microbial biofilm, *Escherichia coli*

1. Introduction

Biofilm formation attached to the surface of medical devices including indwelling devices is a serious contamination problem. Microorganisms develop biofilm made up of extracellular polymeric substances (EPS) when they irreversibly adhere to surfaces and provide structural matrix. Bioflim-associated microorganisms exhibit different behavior compared to planktonic organisms resulting in a public health problem [1]. Biofilms also frequently appear resistant against host immune defense or medical treatments due to the combination of bacterial characteristics and functions of protective matrices [2]. Investigation and detection of biofilms attached on the medical device surfaces is of great importance.

Several imaging modalities have been adapted for investigation of biofilm growth in biomedical research, for example, laser scanning microscopy [3], optical coherence tomography [4], low-coherence interferometry [5]. Hyperspectral imaging (HSI) has been utilized in many research fields including the biofilm monitoring on agricultural equipments and products [6]. Biofilm growth on stainless-steel surface has been reported [7].

Stainless-steel (SS) is one of the most widely used metallic materials for constructing medical devices due to its resistance to corrosion and heat. Depending on composite materials other than iron that consist SS, such as chromium and nickel, SS can have vastly distinctive material properties. International Organization for Standard (ISO) specifies the requirement on the material composition of SS for surgical and dental instruments in ISO 7153, and for implants in ISO 5832. Type 304 surgical stainless steel, which was used in this study, is an austenitic steel containing 18-20% chromium and 8-10% nickel. Mirror-like polished finish is possible for SS, however, mirror finish is in general accomplished by chromium coating on the surface rather than pure polishing of SS. Brushed finishing of SS is most commonly available.

Titanium (TI) is metallic material widely used for implants due to its immunity to corrosion, bio-compatibility, and strength. The requirement for TI which is used for medical implant is specified in ISO 5832. Although limited to very small application area such as micro-surgical tools, TI is also used for constructing surgical and dental tools. Titanium-alloys (TA) are

Design and Quality for Biomedical Technologies V, edited by Ramesh Raghavachari, Rongguang Liang,
Proc. of SPIE Vol. 8215, 821507 · © 2012 SPIE · CCC code: 1605-7422/12/$18 · doi: 10.1117/12.909980

also widely used for implants and surgical tools. TA contains foreign materials such as aluminum, iron, and niobium. Non-reflecting satin finish is most common for TI and TA.

In this study, we present the monitoring of biofilm growth on SS, TI, and TA surfaces.

2. Experiments

We prepared 5 mm × 25 mm strips of SS (304, brushed), pure TI (grade 2, unfinished), and TA (Ti_6Al_7Nb, unfinished). Digital photograph of the samples is shown in Fig. 1(a). Fine stripes of brushed-finish can be observed from SS, while grainy surface morphology could be observed from the surface of TI and TA strips. Under the fluorescent light, SS distinctively exhibited higher reflectivity compared to TI and TA. Metal strips were cleaned using ethanol and phosphate buffered saline (PBS), and then placed in a beaker filled with Luria Bertani broth (LBB, Sigma-Aldrich L3022), which was the growth media. Nonpathogenic bacteria, *Escherichia coli* (*E. coli*, Invitrogen DH10B), were used in this study to generate biofilm on the metal strips. E. coli strain was inoculated into the LBB, and the samples were incubated at 37 degree Celsius for four days. The growth medium was added every 24 hours. The medium was neither stirred nor flowed during the growth. The beaker was left open. After the growth of biofilm, metal strips were washed by unpressurized flow of PBS at pH 7.4. The samples were placed in a glass-bottom petri dish which is filled with PBS during the observation.

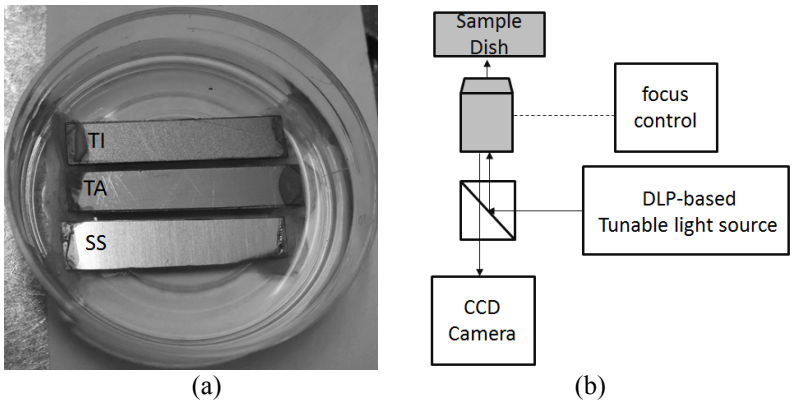

(a) (b)

Fig. 1. (a) Digital photography of metal strips contained in the petri dish filled with PBS; (b) Schematic of the image microscope setup.

The schematic of hyperspectral imaging setup is shown in Fig. 1(b), and the details are described elsewhere [8, 9]. In brief, the imaging system is based on an inverted microscope (Zeiss Axioplan) for real-time monitoring of biofilm growth. However, an upright microscope may serve as well for post-growth observation. A digital light processor (DLP) based tunable light source (Gooch & Housego, OL 490) was coupled to the microscope using a liquid light-guide. Reflectance images of the sample were acquired by an interlaced charge-coupled device (iCCD) camera (Hamamatsu ORCA-2) while the wavelengths of the illumination light were tuned from 400 nm to 700 nm in 10 nm intervals. The spectral width (Full Width at Half Maximum) of the light source was 5 nm. One of the most challenging tasks of the hyperspectral microscopy is to compensate the chromatic aberration from the objective lens. The focus control unit of the microscope was connected to a computer-controlled step-motor, and the correct position of the focus control unit at each wavelength was recorded prior to the sample imaging. During the image acquisition, the position of the objective lens was adjusted to the recorded

focal position prior to each acquisition at different wavelength. Spectral intensity profile of the tunable light source was also compensated similarly. A high-sensitivity low-noise imager such as iCCD is critical for successful hyperspectral imaging because tunable light sources typically exhibit intensity fall-off at the end of the spectral output band.

3. Data Analysis

For analyses of the hyperspectral image data, the size of the region of interest (ROI) needs to be determined first. The background (untreated) metallic surfaces may reflect lights in different directions. This can potentially change the transparent sample spectrum (i.e., biofilms). Fig. 2 shows the ROI microscopic images of the three metal strips acquired using a 4x objective lens with 530 nm illumination.

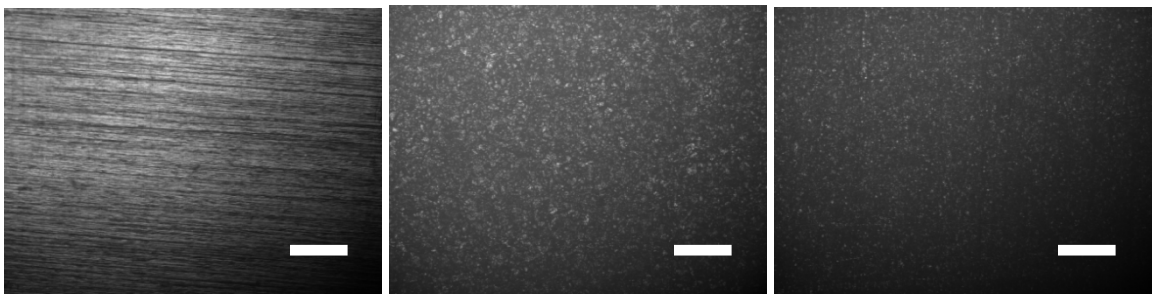

(a) (b) (c)

Fig. 2. Representative ROI microscopy images of the background materials acquired with 530 nm illumination using a 4x objective lens: (a) SS; (b)TI; and (c) TA. Scale bars represent 500 μm.

According to Fig. 2(a), SS surface showed the strongest reflection compared to TI and TA, with directional texture. TI and TA showed similar surface textures as can be seen in Figs. 2(b) and 2(c). However, TI had slightly larger granular texture compared to TA. The spectra of three blank strips of SS, TI, and TA were analysed using different sizes of region-of-interest (ROI), which were shown in Fig. 3.

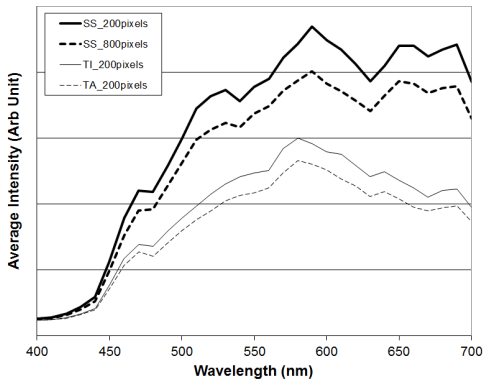

Fig. 3. Background spectra from SS, TI, and TA. For SS, different sizes of ROI were tested to find optimal ROI size.

Three different sizes of ROI were analysed for their background spectra: ROI of square with 100 pixels, 200 pixels, 400 pixels, and 800 pixels of side length out of total 1344 × 1024 pixels of whole images. ROIs were placed from the top left corner of the whole images. In this report, in Fig. 3, 200×200-pixel and 800×800-pixel data for SS are shown in bold solid and dotted lines, respectively. As can be seen for SS in Fig. 3, the shapes of the spectra remained unchanged regardless of the sizes of the ROIs while overall intensity varied depending on the ROI size. Location of the ROI contributes to the overall intensity of the signal due to non-uniform illumination. Non-uniform illumination could be corrected using post-acquisition image processing technique, however, it did not affect the peak locations thus the qualitative data analysis of this study. Same independency of spectrum to the ROI size was confirmed for TI and TA (spectra not shown for brevity). Thus, 200×200-pixel square was chosen to be used as background ROI to determine relative absorbance of the microbial samples formed on the background metallic surfaces in subsequent section. The spectra of TI and TA were almost identical, although they are different from that of SS. The same analyses were repeated for all three metal strips with petri dish filled with PBS and LBB to ensure that spectrum analysis is not affected by factors other than the spectral signature of biofilm itself.

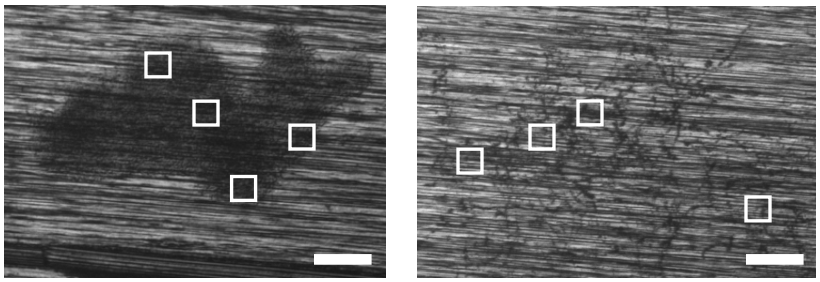

(a) (b)

Fig. 4. ROI microscopy images acquired with 530 nm illumination using the 4x objective lens: (a) *E. coli* colony and (b) biofilm. Scale bars represent 100 μm. White hollow squares represent ROI locations 1 to 4 (from left to right) used in spectral analysis of Fig. 5, respectively for (a) and (b).

Figs. 4(a) and 4(b) show ROI images of *E. coli* colony and biofilm formed on the SS strip under 530 nm illumination. Compared to the cluster of cellular structure observable from E. coli colony in Fig. 4(a), the biofilm clearly reveals the formation of a matrix in Fig. 4(b). To determine the appropriate ROI and spectra for *E. Coli*, a similar procedure used to determined the background spectra above was performed, but with smaller ROIs. Among 5×5-pixel, 20×20-pixel, 50×50-pixel, and 100×100-pixel ROI's, 20×20-pixel ROI produced the most repeatable results.

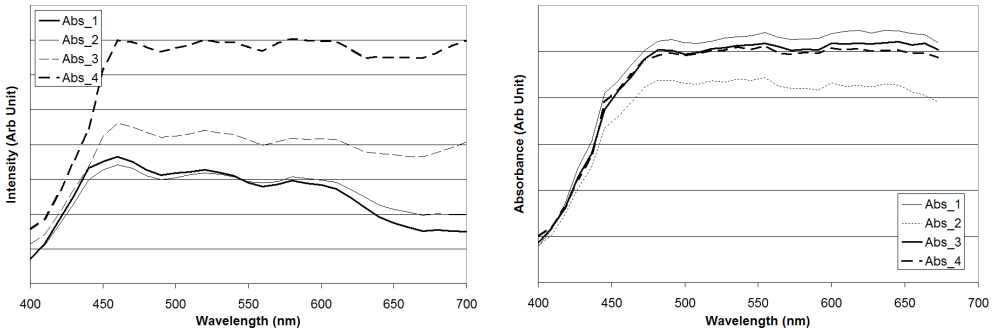

(a) (b)

Fig. 5. Relative absorbance spectra for (a) *E. coli* colony and (b) biofilm measured on four different ROI locations.

Figs. 5(a) and 5(b) show relative absorbance spectra from *E. coli* colony and biofilm, respectively. Spectra were taken from multiple ROIs of 20×20-pixel square at different locations. Relative absorbance was calculated as such:

$$\text{Relative Absorbance} = \frac{\text{Background Intensity - ROI Intensity}}{\text{Background Intensity}} \quad (1)$$

The results show distinctive differences in the absorbance between *E. coli* colony and biofilm: the colony revealed absorption peaks at 460 nm, 520 nm, 580 nm, and 620 nm, while the peaks from biofilm were observed at 470 nm, 560 nm, and 620 nm. The difference in the absorbance between colony and biofilm indicates that biofilm is comprised of materials such as EPS which is different from that of colony. The data were collected from 400 nm to 700 nm with 10 nm spectral interval, thus the spectral bandwidth limited to 10 nm may be the limiting factor for this study. However, it is believed that the absorption signals from very thin transparent layer of E. coli colony and biofilm were not strong enough to produce distinctively high absorption peaks.

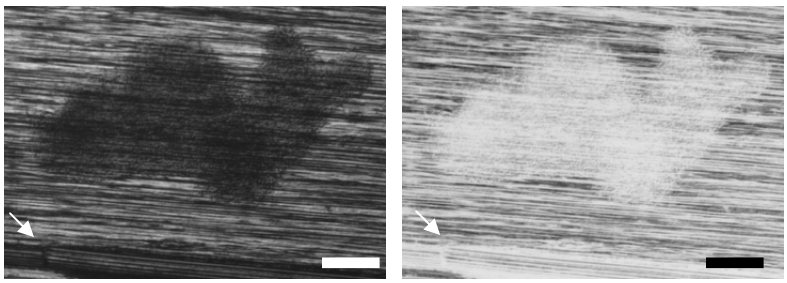

(a) (b)

Fig. 6. Images of E. coli colony on SS: (a) reflectance image under 530 nm illumination; (b) first (score) principal component image obtained from principal component analysis in contrast to 530 nm illumination image. Scale bars represent 100 μm. Arrows indicate the location of scratch marks.

Principal component analysis (PCA) was performed on both *E. coli* colony and biofilm data using in-house analysis software. First principal component (score) images provided most distinguishable contrast for the colony and biofilm. However, irregular reflection from scratch marks (indicated by arrows in Fig. 6) of SS could not be distinguished from *E. coli* colony. The

scratch marks were introduced before the biofilm growth for easiness of finding center location of the metal strip when observed under a microscope. In Fig. 6, although *E. coli* colony {Fig. 6(a)} could be clearly distinguished from the background in the first principal component image {Fig. 6(b)}, intentional scratch mark (thick horizontal line at the bottom of Fig. 6) could not be distinguished from *E. coli* colony. Note that the eigenvectors for the first principal component are close to the original spectra, thus the first principal component image shown in Fig. 6(b) is similar to the negative image of Fig. 6(a).

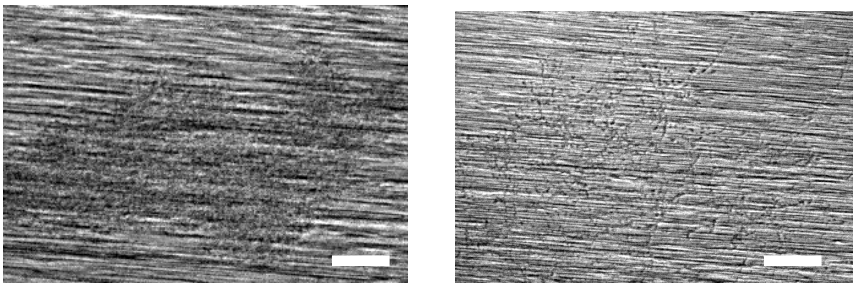

(a) (b)

Fig.7. Two-band difference images of (a) E. coli colony and (b) biofilm. Scale bars represent 100 μm.

To enhance the spectral differences between the background materials and *E. coli*, two-band difference images were constructed for further evaluation. Shown in Figs. 7(a) and 7(b) are two-band difference images of *E. coli* colony and biofilms, respectively. Local peaks were observed at 620 nm for both *E. coli* colony and biofilm as shown in the spectra of Figs. 5(a) and 5(b). In contrast, all the background materials exhibited a valley at 640 nm. Thus, the difference images (620 nm – 640 nm) where 620 nm as the signal and 640 nm as the background, constructed images seen in Fig. 7. As can be seen from the images, *E. coli* colony and biofilm were clearly distinguished from the background. Also, different from the PCA image shown in Fig. 6(b), Fig. 7(a) did not reveal the horizontal scratch mark at the bottom as the signal. No colony or biofilm formations were observed from TI and TA, which is predicted that the surface morphology of TI and TA contribute to the resistance to formation of biofilm. However, further study will be performed in the future to find the explanation.

4. Conclusion

Formations of biofilms on different types of metals used in medical devices were investigated using a microscopic hyperspectral imaging technique. Stainless-steel, titanium, and titanium-alloy, three most common metals used for medical devices were tested. Non-pathogenic strain, *E. coli*, was used to grow biofilm on three different metal strips. Using the microscopic hyperspectral reflectance imaging, biofilm formation was distinguished from the background stainless-steel surface. However, biofilm formation was not observed on titanium and titanium-alloy surfaces. Different materials show different biofilm formation, which is believed to be due to the different surface morphology. Further study will be performed to find the reason for TI and TA not having biofilm formation on the surface.

Disclaimer: The mention of commercial products, their sources, or their use in connection with material reported herein is not to be construed as either an actual or implied endorsement of such products by the Department of Health and Human Services. Certain commercial equipment, instruments, or materials are identified in this manuscript. Such identification does not imply

recommendation or endorsement by the National Institute of Standards and Technology, nor does it imply that the materials or equipment identified are necessarily the best available for the purpose.

Acknowledgements
The authors thank Drs. Ji Youn Lee and Matthew Clarke at National Institute of Standards and Technology (NIST) for their help on the instrumentation of the hyperspectral microscope and data analysis. This research was supported by the NIST Innovative Measurement Science Program on Optical Medical Imaging. DK thanks Drs. Ilko K. Ilev, Xin Tan, Victorica Hitchins, and Shani Haugen for their initial discussion on the biofilm growth.

References
1. Donlan, R.M., "Biofilms and device-associated infections," Emerging Infectious Diseases 7(2), 277-281 (2001).
2. Anderson, G.G. and O'Toole, G.A., "Innate and induced resistance mechanisms of bacterial biofilms," Curr. Top. Microbiol. Immunol. 322, 85-105 (2008).
3. Lawrence, J.R., Koreber, J.D., Hoyle, B.D., Costerton, J.W., and Caldwell, D.E., "Optical sectionning of microbial biofilms," J. Bacteriol. 173, 6558-6567 (1991).
4. Xi, C., Marks, D., Schlachter, S., Luo, W., and Boppart, S.A., "High-resolution three-dimensional imaging of biofilm development using optical coherence tomography," J. Biomed. Opt. 11, 034001 (2006)
5. Nguyen, C.T., Tu, H., Chaney, E.J., Stewart, C.N., and Boppart, S.A., "Non-invasive optical interferometry for the assessment of biofilm growth in the middle ear," Biomed. Opt. Express 1, 1104-1116 (2010).
6. Jun, W., Kim, M.S., Cho, B.K., Millner, P.D., Chao, K., and Chan, D.E., "Microbial biofilm detection on food contact surfaces by macro-scale fluorescence imaging," J. Food Eng. 99, 314-322 (2010).
7. Jun, W., Kim, M.S., Lee, K., Millner, P., and Chao, K., "Assessment of bacterial biofilm on stainless steel by hyperspectral fluorescence imaging," Sens. Instrumen. Food Qual. 3, 41-48 (2009).
8. Clarke, M., Litorja, M., Allen, D., Samarov, D., and Hwang, J., "Characterization of hyperspectral imaging and analysis via microarray printing of dyes," *Proc. SPIE* 7891, 7891W1-8 (2011)
9. Lee, J.Y., Clarke, M., Tokumasu, F., Lesoine, J.L., Allen, D.W., Chang, R.C., Litorja, M., and Hwang, J., "Absorption-based Hyperspectral Imaging and Analysis of Single Erythrocytes," IEEE J. Select Top Quant Electr 99, 1-10 (2011).